CFD Analysis of Premixed Methane Chlorination Reactors with Detailed Chemistry

Venkatramanan Raman* and Rodney O. Fox

Department of Chemical Engineering, Iowa State University, Ames, Iowa 50014-2230

Albert D. Harvey and David H. West

The Dow Chemical Company, Freeport, Texas 77541-3257

With the implementation of efficient algorithms for the accurate calculation of reaction source terms, computational fluid dynamics (CFD) is now a powerful tool for the simulation and design of chemical reactors with complex kinetic schemes. The example studied in this work is the methane chlorination reaction for which the detailed chemistry scheme has 152 reactions and 38 species. The adiabatic, jet-stirred chlorination reactor used for the CFD simulations is an insulated right cylinder with a coaxial premixed feed stream at one end. In order for this reactor to remain lit, recirculation of hot products is crucial, and hence, reactor stability is sensitive to both macroscale and microscale mixing. By neglecting density variations, a Lagrangian composition probability density function (PDF) code with a novel chemistry tabulation algorithm (*in-situ* adaptive tabulation or ISAT) for handling complex reactions is used to simulate the species concentrations and temperature field inside of the reactor. In addition, a reduced mechanism with 21 reactions and 15 species is tested for accuracy against the detailed chemistry scheme, a simplified CSTR model is used to illustrate the shortcomings of zero-dimensional models, and a pair-wise mixing stirred reactor (PMSR) model is used to show the stabilizing effect of micromixing on reactor stability. The CFD simulations are generally in good agreement with results from pilot-scale reactors for the outlet temperature and major species.

Introduction

Gas-phase chlorination of hydrocarbons is a commercially important process used for the production of chlorinated derivatives (e.g., methyl chloride, methyl dichloride, and chloroform).[1] These chlorinated products have a variety of applications as industrial solvents, intermediates, and environmentally friendly refrigerants.[2] In the present study, methyl chloride is used as the primary feed, and chloroform is the desired product. Plant-scale reactors typically operate in either premixed or partially premixed adiabatic mode, with the inlet feed jets used to enhance turbulent mixing. The free-radical reactions, however, give rise to a host of secondary products that are difficult to separate. Using methyl chloride as the feed, the maximum yield of desirable products occurs at around 700−740 K. At higher temperatures, the primary products rapidly pyrolyze to a wide range of chlorinated alkenes, and eventually reactor fouling due to carbon deposition can become a problem. The detailed kinetic scheme (reported elsewhere[3,11]) used in this work involves 38 species and 152 reactions.[3] A 21-step reduced scheme with 15 species is also used in the CFD simulations (see Tables 1 and 2).

The modeling of thermochlorination reactors is difficult because of the strong coupling between the turbulent flow and reaction processes. However, faster computers and more efficient algorithms have made such simulations considerably easier.[4−6] Although several authors have reported[7] successful CFD simulations of methane chlorination reactors, most studies have been limited to smaller reaction schemes or one-dimensional models. In general, previous studies have concluded that, unless a detailed kinetic scheme is employed, CFD does a poor job of predicting finite-rate chemistry effects, minor species formation, and reactor extinction. In addition, most CFD simulations have not accounted for micromixing effects which are known to affect reaction rates and, hence, reactor performance.

Table 1. Chemical Species

primary species	HCl	Cl_2	CH_3Cl
	CH_2Cl_2	$CHCl_3$	CCl_4
secondary species	$CHCl_2-CH_2Cl$	CCl_3-CCl_3	CCl_3-CH_2Cl
	CCl_3-CHCl_2	$CHCl_2-CHCl_2$	$Cl^\bullet$
	$CHCl_2^\bullet$	$CCl_3^\bullet$	$CH_2Cl^\bullet$

Table 2. Twenty-One-Step Reaction Scheme

	reaction	A_n	E_n
1	$Cl_2 \rightleftharpoons 2Cl^\bullet$	0.185E+13	0.580E+5
2	$CH_2Cl_2 \rightleftharpoons CH_2Cl^\bullet + Cl^\bullet$	0.1E+17	0.811E+5
3	$CHCl_2-CH_2Cl \rightleftharpoons CHCl_2^\bullet + CH_2Cl^\bullet$	0.1E+16	0.884E+5
4	$CHCl_3 \rightleftharpoons CHCl_2^\bullet + Cl^\bullet$	0.1E+17	0.776E+5
5	$CHCl_2-CHCl_2 \rightleftharpoons 2CHCl_3^\bullet$	0.1E+16	0.824E+5
6	$CCl_3-CCl_3 \rightleftharpoons 2CCl_3^\bullet$	0.1E+16	0.714E+5
7	$CCl_3-CH_2Cl \rightleftharpoons CCl_3^\bullet + CH_2Cl^\bullet$	0.1E+16	0.827E+5
8	$CCl_3-CHCl_2 \rightleftharpoons CCl_3^\bullet + CHCl_3^\bullet$	0.1E+16	0.759E+5
9	$CCl_4 \rightleftharpoons CCl_3^\bullet + Cl^\bullet$	0.1E+17	0.709E+5
10	$CH_3Cl + Cl^\bullet \rightleftharpoons CH_2Cl^\bullet + HCl$	0.1E+14	0.460E+3
11	$CH_2Cl_2 + Cl^\bullet \rightleftharpoons CHCl_2^\bullet + HCl$	0.1E+14	0.460E+3
12	$CH_2Cl_2 + CH_2Cl^\bullet \rightleftharpoons CHCl_2^\bullet + CH_3Cl$	0.3E+12	0.110E+5
13	$CH_2Cl_2 + Cl^\bullet \rightleftharpoons CH_2Cl^\bullet + Cl_2$	0.1E+15	0.224E+5
14	$CHCl_3 + Cl^\bullet \rightleftharpoons CCl_3^\bullet + HCl$	0.1E+14	0.460E+3
15	$CHCl_3 + CH_2Cl^\bullet \rightleftharpoons CCl_3^\bullet + CH_3Cl$	0.3E+12	0.110E+5
16	$CHCl_3 + CHCl_2^\bullet \rightleftharpoons CCl_3^\bullet + CH_2Cl_2$	0.3E+12	0.110E+5
17	$CHCl_3 + Cl^\bullet \rightleftharpoons CHCl_2^\bullet + Cl_2$	0.1E+15	0.189E+5
18	$CHCl_3 + CH_2Cl^\bullet \rightleftharpoons CHCl_2^\bullet + CH_2Cl_2$	0.3E+12	0.110E+5
19	$CCl_4 + Cl^\bullet \rightleftharpoons CCl_3^\bullet + Cl_2$	0.1E+15	0.122E+5
20	$CCl_4 + CH_2Cl^\bullet \rightleftharpoons CCl_3^\bullet + CH_2Cl_2$	0.3E+12	0.110E+5
21	$CCl_4 + CHCl_2^\bullet \rightleftharpoons CCl_3^\bullet + CHCl_3$	0.3E+12	0.110E+5

* Author to whom correspondence should be addressed.

10.1021/ie001033q CCC: $20.00
Published on Web 04/27/2001

Thus, for accurate predictions of minor species and studies of reactor stability, full probability density function (PDF) methods should be employed because of their ability to account for turbulence−chemistry interactions by treating complex reactions without modeling assumptions.[6,8]

In a CFD simulation, continuity and momentum transport equations of the form

$$\frac{\partial \rho}{\partial t} + \frac{\partial}{\partial x_i}(\rho u_i) = 0 \tag{1}$$

and

$$\frac{\partial \rho u_i}{\partial t} + \frac{\partial \rho u_i u_j}{\partial x_i} = \frac{\partial}{\partial x_j}\left(\mu \frac{\partial u_i}{\partial x_j}\right) - \frac{\partial P}{\partial x_i} \tag{2}$$

are solved for the flow field, and a species transport equation of the form

$$\frac{\partial \rho \phi}{\partial t} + \frac{\partial \rho u_i \phi}{\partial x_i} = \frac{\partial}{\partial x_i}\left(\rho D \frac{\partial \phi}{\partial x_i}\right) + \rho \mathbf{S}(\phi) \tag{3}$$

is solved for each species in the kinetic scheme. At high Reynolds numbers, a turbulence model is required to represent the flow field. In this work, our principal interest is the effect of flow on detailed chemistry. Thus, we neglect density variations and employ a relatively simple turbulence model that predicts the mean velocity $\langle u_i \rangle$, the turbulent diffusivity D_T, and a turbulence time scale $\tau_u = k/\epsilon$. These fields are required as input to the full PDF code for the simulation of the turbulent transport of the chemical species.[6] In the more general case of a variable-density flow, a hybrid CFD−PDF approach is used where in the mean density field is found from the PDF code. An iteration procedure is then required to find the mean velocity. In this work, we neglect density variations in order to focus on the issues associated with the chemical source term.

Using a fractional time-stepping algorithm,[9] the chemical source term $\mathbf{S}(\phi)$ can be isolated from the convection and diffusion terms in eq 3. The convection and diffusion terms are simulated using a full PDF method, as described in detail elsewhere.[6] The contribution due to the chemical source term results in a set of nonlinear, stiff ordinary differential equations (ODEs) of the form

$$\frac{\mathrm{d}\phi}{\mathrm{d}t} = \mathbf{S}(\phi) \tag{4}$$

where the chemical source term is given by

$$S_\alpha(\phi) = [\sum_{i=1}^{n_r} (v_{\alpha i}^{r} - v_{\alpha i}^{f}) R_i(\phi)] \tag{5}$$

and $R_i(\phi)$ is the reaction rate corresponding to the ith reaction. The source term for the temperature is derived from an enthalpy balance equation and has the form

$$S_{n_s+1}(\phi) = -\sum_{\beta=1}^{n_s} h_\beta(T)\, S_\beta(\phi) \tag{6}$$

where h_β is the specific enthalpy of the βth chemical species. In a typical full PDF simulation, eq 4 must be solved on the order of 10^9 times and represents the major computational cost.

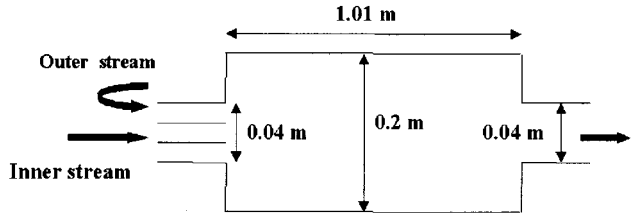

Figure 1. Schematic diagram of jet-stirred reactor.

As mentioned above, the calculation of the source terms in the fractional time-stepping method is a major bottleneck in the simulation process. The simplest method for solving eq 4 is by direct integration (DI). However, because this involves a system of stiff ODEs and also because of the large number of variables involved, it is computationally prohibitive. In a typical full PDF simulation, about 10^6 DIs for around 10^3 time steps must be done, which theoretically would take at least 10^7-10^8 s (3.17 years!). In some cases where DI is not tractable, precomputed chemical look-up tables can be used. These tables store the DI results over the entire composition space, and the result of the computation during the simulation is obtained by multilinear interpolation.[6] This method works well for kinetic schemes involving low numbers of species (e.g., less than six). However, for the detailed chemistry scheme with 38 species considered in this work, the storage space required for even reasonable accuracy (around 39×100^{39} real numbers) is infeasible. Nevertheless, the idea of limiting the number of DIs by using tabulated values instead of repeating the computation is extremely useful. One such method, *in-situ* adaptive tabulation (ISAT), is used in this work.[10] Instead of computing the entire composition space, ISAT computes and stores only those points that are needed in a particular simulation. These points are stored in the form of a binary tree data structure that recursively divides the accessed region into finite tractable subspaces. An ellipsoid of accuracy is defined for each subspace within which linear interpolation can be carried out with user-defined error tolerances. The applicability of ISAT to chlorination chemistry has been investigated elsewhere.[11] The error tolerance parameter for this particular study was set in the range $10^{-2} \le \epsilon \le 10^{-1}$.

Reactor Configuration

Industrial gas-phase chlorination processes typically use coaxial, jet-stirred reactors similar in geometry to the one represented in Figure 1. This reactor has two inlet streams that feed a fixed ratio of organics to chlorine. Although complete premixing is desired, in industrial reactors, the two streams are not completely premixed. The degree of mixing is thus an important aspect of the reactor performance. Here, however, we assume complete premixing as an ideal case and analyze reactor performance based on this assumption. (Studies with nonpremixed feed streams will be reported elsewhere.) In this work, the premixed inlets have identical inlet velocities of 3.11 m/s which corresponds to a reactor residence time of 7.5 s. The feed streams have 25% chlorine, 36% methyl chloride, and 39% methyl dichloride by mass. The inlet temperature is set at 323 K. The feed jet diameters are adjusted to obtain equal velocities. (The effect of unequal velocities is also of interest and will be reported elsewhere.) The flow fields exhibit special characteristics that are critical to sustaining the

reaction. The incoming coaxial jets create a flame-like structure that transports the reactants inside the reacting zone. Mixing occurs primarily in the high-shear region surrounding the interface of the primary jets. The penetration of the reactants deep inside the reactor facilitates secondary and tertiary chlorination. The chlorination reaction is highly exothermic and, like combustion flames, stays lit only above a critical temperature. Hence, the feedback of enthalpy to the incoming cold feed streams is an essential feature of the flow. The rate of heat transfer, as well as the location of the reattachment point of the recirculation zone, is an important parameter in determining the stability of the reactor. The accurate determination of the low Reynolds number recirculating flow is critical for obtaining accurate predictions for chemical species distributions inside the reactor. Indeed, it has been found that relatively small variations in the degree of flow recirculation will result in reactor extinction. To better understand the role of micromixing, we first look at results for simplified reactor models that ignore spatial gradients at large scales.

Results from Simplified Reactor Models

Traditionally, a simple continuous stirred tank reactor (CSTR) model and/or a plug-flow reactor (PFR) model with recycle have been used to understand chlorination reactor performance. In fact, under certain operating conditions, these models are quite accurate in providing outlet species concentrations. In these studies, highly simplified reaction mechanisms (typically involving a chlorine disassociation step) have been used to determine the extent of reaction.[12] Here, we begin by implementing detailed chemistry in two such simple models [namely, the CSTR and the pair-wise mixing stirred reactor (PMSR) models] and neglect density variations. In comparisons with the CFD results presented later, the reader should note that the CSTR model is analogous to a single-particle PMSR model and that both the CSTR and PMSR models neglect spatial variations in the mean species concentrations.

The CSTR model for constant density flow is given by

$$\frac{\mathrm{d}\phi}{\mathrm{d}t} = \frac{1}{\tau}(\phi_{\mathrm{in}} - \phi) + \mathbf{S}(\phi) \qquad (7)$$

where ϕ_{in} is the inlet mass fraction/enthalpy vector and τ is the reactor residence time. To be consistent with the CFD simulations, we use operator splitting to separate the reaction term from the inflow−outflow term in eq 7. The residence time and inlet conditions of the CSTR were first set to be the same as for the coaxial jet-stirred reactor ($\tau = 7.5$ s, $T_{\mathrm{in}} = 323$ K). However, for this inlet temperature, increasing the residence time had no effect on reactor performance. (In fact, the inlet temperature $T_{\mathrm{in}} = 323$ K is too low to sustain reactions in a CSTR for this residence time.) The inlet temperature was thus increased, and it was found that, at $T_{\mathrm{in}} = 365$ K (Figure 2), the reactor ignites and remains lit. Using this inlet temperature, increasing the residence time yielded similar results with an ignition at $\tau = 3.85$ s (Figure 3). Although the assumption of complete backmixing is far from reality, these results illustrate the effect of the residence time on reactor stability. In the full-scale reactor, fluid particles have long sojourn times in the recirculation region and short sojourn times in the entrance region. Whether these regions remain lit depends on the extent of back-mixing and the local micromixing times. However, pilot-scale reactors with $\tau = 7.5$ s have been found to remain stable at an inlet temperature of $T_{\mathrm{in}} = 323$ K. Thus, we can conclude that local variations in the extent of mixing will affect reactor dynamics, and these effects must be studied using more detailed flow models.

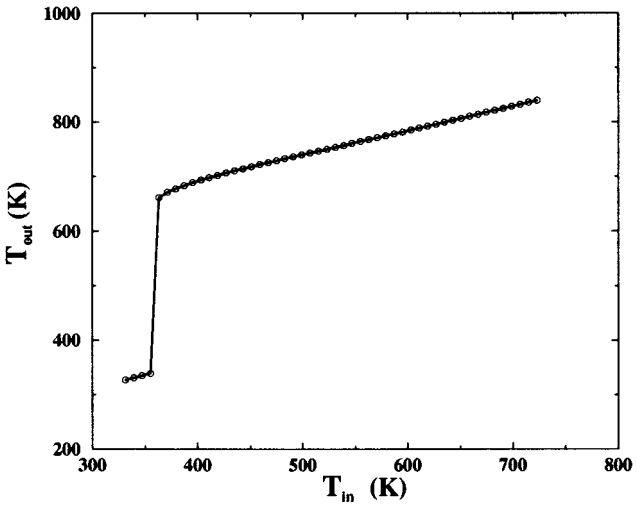

Figure 2. CSTR model: Variation of outlet temperature with inlet temperature at a constant residence time of 7.5 s.

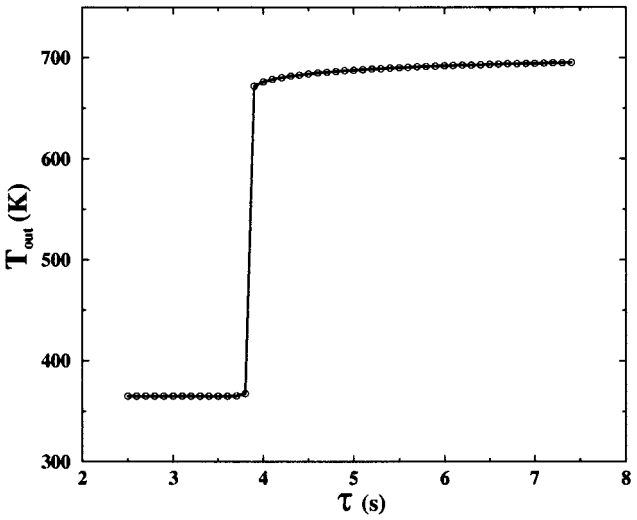

Figure 3. CSTR model: Variation of outlet temperature with residence time at inlet temperature of 365 K.

The PMSR model[10] is an extended version of the CSTR model with a finite number of fluid particles that evolve in composition space by reaction and micromixing. The particles are paired, and the micromixing model is applied between the partners in every pair. The particles exchange partners based on a fixed pairing time and relax to the mean composition (of the partners) based on a predetermined micromixing time scale τ_{m}. The PMSR model reduces to a CSTR as the micromixing and pairing time approach zero. (Further details on the PMSR model can be found elsewhere.[10,11]) For the jet-stirred reactor, the "average" micromixing time (volume average of k/ϵ) was found from the turbulence model to be around $\tau_{\mathrm{m}} = 0.558$ s. The pairing time was (arbitrarily) set equal to the micromixing time. With the residence time set to $\tau = 7.5$ s and $T_{\mathrm{in}} = 323$ K, it was found that the PMSR model yields a stable reacting steady state. The assumption of finite-rate micromixing

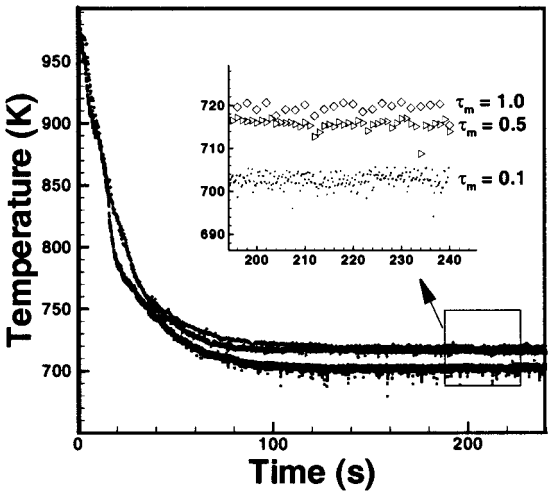

Figure 4. PMSR model: Effect of micromixing time on final temperature. Residence time is 7.5 s, with an inlet temperature of 323 K.

(as opposed to infinite-rate micromixing) thus suffices to change the behavior of the reactor. The micromixing time was then varied, and it was found that the reacting steady-state temperature decreased with decreasing micromixing time (Figure 4) until the reactor eventually extinguished. Although the PMSR model does predict a reacting steady state at the desired inlet temperature and residence time, it cannot predict changes in reactor stability due to variations in the flow field (e.g., changes in local shear rate due to variations of the feed jet radius). To address such questions, it is necessary to predict both the detailed flow field and species concentration fields. This can be done using CFD simulations of the jet-stirred reactor with detailed chemistry.

Results from CFD Simulations

In this work, CFD simulation of the jet-stirred chlorination reactor is done with a Lagrangian PDF method.[6] The composition PDF code requires a stationary flow field obtained from a CFD turbulence model. Here, the flow is assumed to be at steady state and incompressible. (Effects of density variations on reactor performance will be reported elsewhere.) The velocity, pressure, and turbulent kinetic energy fields are precomputed using a finite-volume Navier−Stokes solver in generalized coordinates. The flow is solved for an axisymmetric case using a $k-\omega$ turbulence model. The cell-centered velocity, turbulent kinetic energy, and energy dissipation fields are input to the composition PDF code. From these fields, the turbulent diffusivity and the local mixing times are computed (Figure 5). In the composition PDF codes, the flow domain is assumed to contain a finite number of stochastic particles, which move in physical space using the flow profiles from the

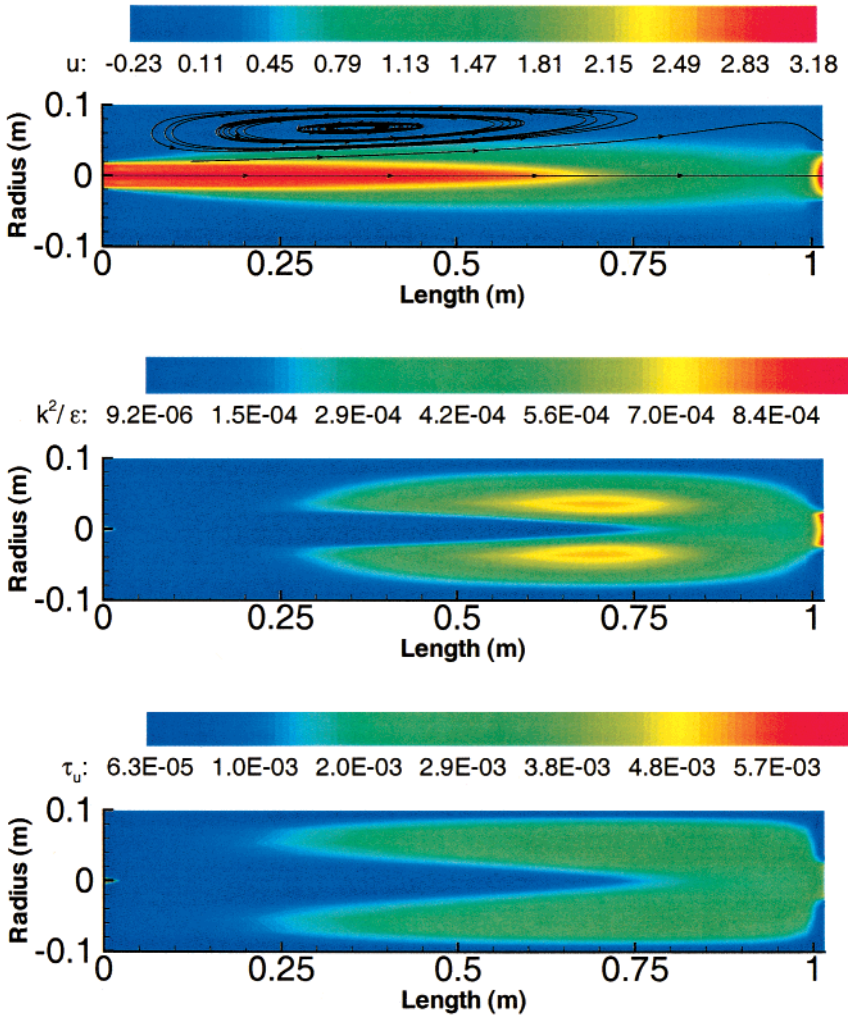

Figure 5. Mean velocity (top), turbulent diffusivity (middle), and local mixing time (bottom) profiles obtained from a $k-\omega$ turbulence model with a 15-species reaction mechanism.

Table 3. ISAT Performance Statistics

method	error tolerance	CPU (min)	no. of records	no. of DI	outlet temp (K)
DI	10^{-8}	78	–	240 000	718
ISAT	10^{-3}	25	8056	23 453	719
ISAT	10^{-2}	10	2002	11 244	719.5
ISAT	10^{-1}	3.5	336	3179	716

turbulence models and evolve in composition space by reaction and micromixing. Usually, the particles are evolved over 3−4 residence times to obtain steady-state profiles. The micromixing in each cell is accounted for by a simple interaction by exchange with the mean (IEM) model.[8] This model assumes a linear rate for micromixing that is proportional to the distance between the mean composition vector in a cell and the particle composition vector. The micromixing rate involves a time constant that is taken to be proportional to the turbulence time scale τ_u. A fixed time step is used with fractional time stepping to facilitate the use of ISAT to calculate the reaction source term. On average, 80−120 particles per grid cell are employed on a 40 × 28 axisymmetric Cartesian grid. The grid has nonuniform cells with denser grid points near the entrance region to capture the interface of the two feed jets. The simulations were performed on a 266 MHz Alpha workstation.

Simulation of the initial transient regime requires a large number of records in the ISAT binary tree, and consequently, the storage memory requirement is relatively large. Individual studies with a PMSR model were carried out to test the validity of the parameters used in ISAT (see Table 3). It was found that, even at an error tolerance value of $\epsilon_{tol} = 10^{-1}$, the results from interpolation are quite accurate. The use of ISAT was found to yield significant speedups (see Table 4). It was also found that the speedup is nonlinear with respect to the number of chemical source term calls. The use of the detailed 38-species mechanism further slowed the simulation as compared to the reduced 15-species mechanism. Overall, despite using efficient algorithms for evaluating the reaction term, the computational time was relatively high. Thus, a multiprocessor parallel independent simulation was carried out to accelerate the calculation. It was found that the reaction computation took nearly 99% of all computation time, and hence, a MPI-based parallel code was implemented to divide the computational load more evenly among the processors. In this code, the reaction computation was parallelized while each processor carried the entire simulation domain. The highly vectorizable nature of the Monte Carlo method, along with the reduced interprocessor communications, yielded nearly linear scale-up. It was also found that DI scaled linearly, but the use of a nonlinear data structure in the form of a binary tree slowed the scale-up with ISAT. Hence, the observed speedup was significantly lower for ISAT than DI, even though the wall time for the ISAT simulations was very low as compared to that for DI.

Three different simulation conditions were tested. Two of these used the detailed 38-species mechanism, whereas the third used the reduced 15-species mechanism. The mixing time was found to be low near the entrance region because of higher velocities (Figure 5). In the detailed chemistry simulations, the micromixing parameter (C_ϕ) was varied to analyze the effect of micromixing on reaction. A large C_ϕ value forces the composition of the particles inside a grid cell to the mean

Table 4. PDF Simulation Statistics

method	no. of CPUs	source calls per Δt	wall time[a]	C_ϕ	no. of records	n_s
DI	1	560	23.5 h	∞	–	15
ISAT	1	560	7.4 h	∞	707	15
DI	4	25 000	6.3 days	1	–	15
ISAT	1	25 000	18.1 h	1	930	15
ISAT	1	25 000	4 days	1	2106	38

[a] Wall time refers to real time (as if measured by a wall clock) required for the simulation.

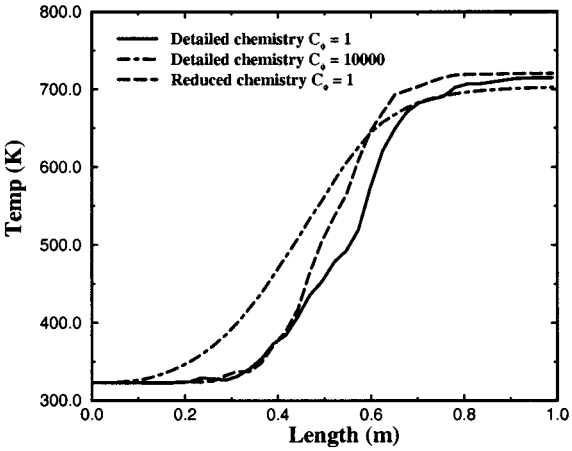

Figure 6. Comparison of time-averaged center-line temperature profiles for detailed and reduced chemistry with different micromixing parameters after three residence times.

value, thereby approximating a finite-volume code that neglects micromixing. (Note, however, that the spatial transport algorithm used in the Lagrangian PDF code is more accurate for the same grid resolution than the method used in the CFD code.[13]) It was found that (Figure 6) the use of a micromixing model results in a higher outlet temperature (714 K) as compared to that of a completely micromixed reactor (703 K). This shows that the implementation of even a simple micromixing model makes a definite difference in the reactor performance predictions. It can also be seen that, although the two different mechanisms (detailed and reduced chemistry) yield similar temperature and species profiles, the reduced chemistry produces a higher temperature in the diffuse reaction zone. Nevertheless, the predicted reactor outlet temperature and species concentrations agree closely, although simulation with the detailed chemistry resulted in a slightly more diffuse reaction zone. The computational time for the detailed chemistry was approximately five times higher than that for the reduced chemistry. In both cases, the outlet temperature was around 715 K, and the concentration of chloroform in the product was between 12 and 14% by mass. The temperature and species profiles (Figure 7) indicate the presence of a characteristic reaction zone that surrounds the inlet jet. The chlorine profile and its penetration into the reactor determine the nature and extent of the reaction. Rapid depletion of chlorine can lead to regions of high temperature that promote disassociation of chloroform and methyl dichloride. However, a higher chlorine content near the outlet of the reactor can cause further chlorination of the desired products, resulting in increased production of carbon tetrachloride and other secondary products. The maximum chloroform yield is known to occur around 700−

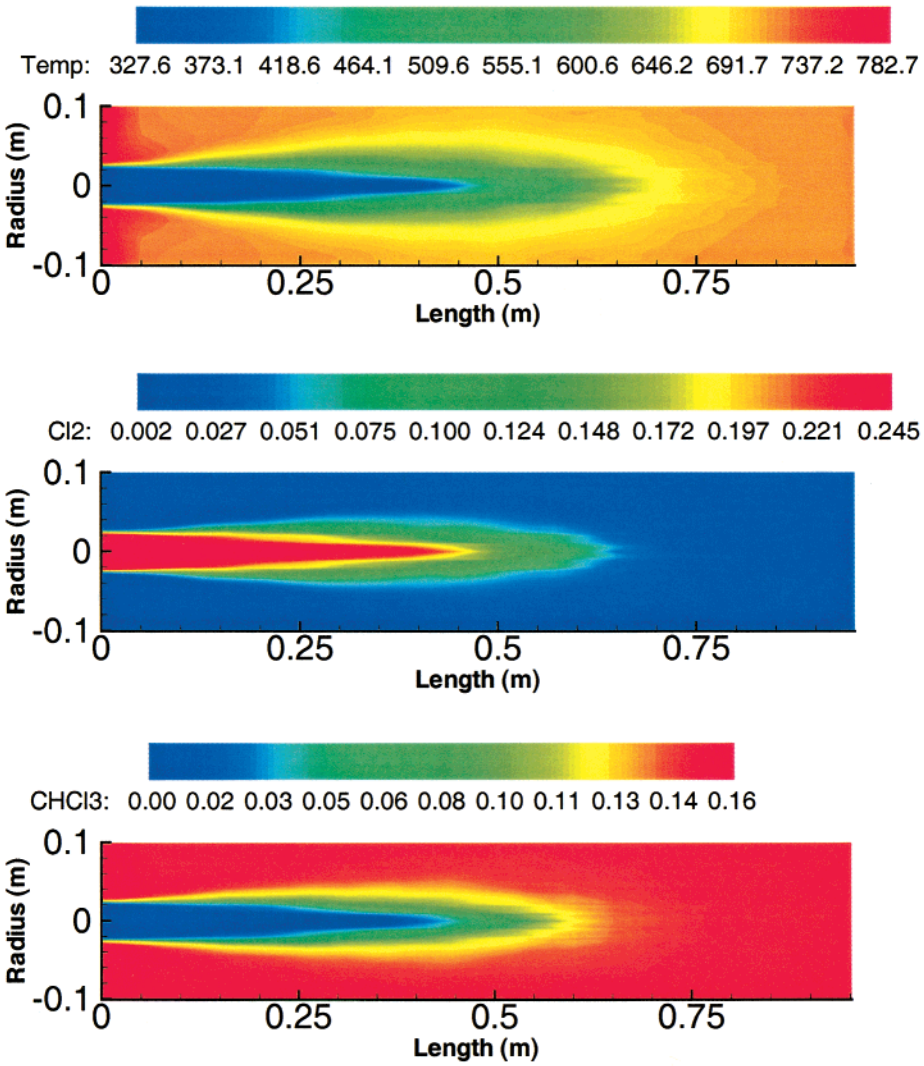

Figure 7. Temperature (top), chlorine (middle), and chloroform (bottom) profiles with detailed chemistry simulated using a composition PDF method.

740 K, and the premixed jet-stirred reactor configuration is quite suitable for obtaining this temperature range.

Conclusions

The Lagrangian composition PDF method is able to predict outlet temperatures and species distributions with reasonable accuracy when compared to data from industrial chlorination reactors. The reduced mechanism captures the essential dynamics of the reactor and agrees closely with results obtained using the detailed chemistry. Hence, the reduced chemistry is useful in estimating reactor performance. The reactor flow configuration is critical in sustaining the reactor. The proper choice of inlet velocities is necessary to keep the recirculation large enough to increase enthalpy backflow, but at the same time avoid formation of a large dead zone that might result in either a reaction runaway or extinction through the presence of stagnant reacting fluid that could be considered more like a batch reactor. Although not studied in detail in this work, the interface between the jets improves mixing, and hence, the effective ratio of the jet velocities is an important factor in determining the mixing zone. It is evident that the reaction zone itself is situated in this high-shear layer. The jet velocity ratio of 1.0 used in this work results in a restricted mixing zone as well as a limited reaction zone that is characterized by a sharp temperature gradient. The jet velocities also depend on the inlet pipe diameters which indirectly affect the positioning of the mixing zone because the interface of the jets itself is moved when the pipe diameter is changed. The concentration of methyl dichloride was found to increase locally near the mixing zone, indicating that most of the primary and secondary chlorination occurs in the mixing zone. Again, these reactions are highly exothermic and the presence of the back-mixing zone helps carry the enthalpy back to the inlet jets. The flow profiles compared with the final species profiles show the distinct tendency of the reaction to follow the fluid flow. This hints at the use of flow to control the reaction. Industrial reactors have been found to exhibit nonlinear behavior, such as extinction, re-ignition, and sustained oscillations, which are not predicted by our study (probably because of the assumption of constant-density flow in an overall exothermic system). Future work aims at the development of a hybrid finite-volume (FV)−PDF approach to account for the effects of density variations on the flow field.

Acknowledgment

We gratefully acknowledge support from the U.S. National Science Foundation (CTS-9996242) and the Dow Chemical Company.

Notation

n_s = number of species
n_r = number of reactions
ϕ = composition vector of length $n_s + 1$
$\mathbf{S}(\phi)$ = source term vector of length $n_s + 1$
$\mathbf{R}(\phi)$ = reaction rate vector of length n_r
h_β = specific enthalpy of the βth species
$\upsilon''_{\alpha i}$ = integer stoichiometric coefficient for the reverse reaction
$\upsilon'_{\alpha i}$ = integer stoichiometric coefficient for the forward reaction
ϵ = error tolerance
τ = residence time
τ_m = micromixing time
T_{in} = inlet temperature
T_{out} = outlet temperature

Literature Cited

(1) Wiseman, P. *An Introduction to Industrial Organic Chemistry*, 1st ed.; Wiley: New York, 1972.

(2) Reed, D. J. *Encyclopedia of Chemical Technology*, 4th ed.; Kroschwitz, J. I., Executive Ed., Howe-Grant, M., Ed.; Wiley: New York, 1991.

(3) Tirtowidjo, M. Fundamental Kinetic Modeling of Industrial Reactors. AIChE Annual Meeting, Los Angeles, CA, Nov 1997; Paper 78b.

(4) Deutschmann, O.; Schmidt, L. D. Modeling the Partial Oxidation of Methane in a Short-Contact-Time Reactor. *AIChE J.* **1998**, *44*, 2465.

(5) Kolhapure, N.; Fox, R. O. CFD Analysis of Micromixing Effects on Polymerization in Tubular Low-Density Polyethylene Reactors. *Chem. Eng. Sci.* **1999**, *54*, 3233.

(6) Tsai, K.; Fox, R. O. PDF Modeling of Turbulent-Mixing Effects on Initiator Efficiency in a Tubular LDPE Reactor. *AIChE J.* **1996**, *42*, 2926.

(7) Acharya, S.; Jang, D. S.; West, D. H.; Hebert, L. A. A Moment Closure Method for Modeling a Multistep Chlorination Reaction, AIChE Spring National Meeting, Houston, TX, March 1991; Paper 33a.

(8) Pope, S. B. PDF Methods for Turbulent Reactive Flows. *Prog. Energy Combust. Sci.* **1985**, *11*, 119.

(9) Yang, B.; Pope, S. B. An Investigation of the Accuracy of Manifold Methods and Splitting Schemes in the Computational Implementation of Combustion Chemistry. *Combust. Flame* **1998**, *112*, 16.

(10) Pope, S. B. Computationally Efficient Implementation of Combustion Chemistry Using In Situ Adaptive Tabulation. *Combust. Theory Modell.* **1997**, *1*, 41.

(11) Shah, J. J.; Fox, R. O. Computational Fluid Dynamics Simulation of Chemical Reactors: Application of In Situ Adaptive Tabulation to Methane Thermochlorination Chemistry. *Ind. Eng. Chem. Res.* **1999**, *38*, 4200.

(12) West, D. H.; Hebert, L. A.; Pividal, K. A. Detection of Quenching and Instability in Industrial Chlorination Reactors, Fall National AIChE Meeting, Dallas, TX, Nov 1999.

(13) Mobus, H.; Gerlinger, P.; Bruggemann, D. Comparison of Eulerian and Lagrangian Monte Carlo PDF Methods for Turbulent Diffusion Flames. *Combust. Flame* **2001**, *124*, 519

Received for review December 1, 2000
Revised manuscript received March 12, 2001
Accepted March 14, 2001

IE001033Q